High Tolerance of Double-Decker Phthalocyanine Towards Molecular Oxygen

Mattia Farronato, Johann Lüder, Danilo Longo, Hervé Cruguel, Marcel Bouvet, Barbara Brena, Nadine Witkowski

High Tolerance of Double-Decker Phthalocyanine Towards Molecular Oxygen

Mattia Farronato,[†] Johann Lüder,[‡a] Danilo Longo,[†] Hervé Cruguel,[†] Marcel Bouvet,[¶] Barbara Brena,[‡] and Nadine Witkowski[*,†]

†*Sorbonne Université, UMR CNRS 7588, Institut des Nanosciences de Paris, 4 Pl. Jussieu, F-75005 Paris, France*

‡*Department of Physics and Astronomy, Uppsala University, Box-516, 75120 Sweden*

¶*Institut de Chimie Moléculaire de l'Université de Bourgogne, UMR CNRS 6302, Université Bourgogne Franche-Comté, F-21000 Dijon, France*

E-mail: nadine.witkowski@sorbonne-universite.fr

Phone: +33 (0)144274342

[a]Current address: Department of Materials and Optoelectronic Science, National Sun Yat-Sen University, Kaohsiung, Taiwan

Abstract

Because organic electronics suffer from degradation inducing oxidation processes, oxygen tolerant organic molecules could solve this issue and be integrated to improve the stability of devices during operation. In this work, we investigate how lutetium double-decker phthalocyanine ($LuPc_2$) reacts towards molecular oxygen and we report microscopic details of its interaction with $LuPc_2$ film by combining X-ray Photoemission Spectroscopy, Near Edge X-ray Absorption Fine Structure Spectroscopy and Density Functional Theory. Surprisingly, $LuPc_2$ molecules are found to weakly physisorb below 120 K and appear rather inert to molecular oxygen at more elevated temperatures. We are able to draw a microscopic picture at low temperature in which oxygen molecules stick on top of the pyrrolic carbon of $LuPc_2$. Our work sheds light on a class of semiconducting molecules, namely double-decker phthalocyanines, that present a high tolerance towards molecular oxygen, opening promising perspectives for the design of stable materials to be applied in the next generation of organic based electronic devices operating under ambient conditions.

Introduction

Recently, devices based on organic electronics have attracted a lot of attention both on the market and in the research laboratories.[1–3] Their advantages versus the inorganic silicon based devices are multiples: they are cheap, flexible, and they offer almost infinite tayloring possibilities making these devices ideal for large scale implementation in urban areas. Among the organic materials used both for research and for devices application, one of the most interesting is represented by phthalocyanines (Pcs) and their derivatives. They are thermally stable, and present interesting electronic and optical properties. For instance, copper phthalocyanine, known as p-type semiconductor, has been extensively studied in organic light-emitting diode (OLED) or in organic photovoltaic cells.[4–6] One of the major drawbacks that hinders phthalocyanine based materials from taking over the market, is their

reduced lifetime originating from photobleaching, exposure to elevated temperature (in the range of 70-100°C) or exposure to reactive gases or radiation. In particular the exposure towards atmospheric gases can cause many different problems as reactivity,[7,8] and even polymerization of the organic material in presence of oxygen at operating temperatures.[9]

In the case of phthalocyanine few studies have been published on its reactivity towards gases as O_2 on FePc,[10] NO_2 on CuPc[11] and NO on CoPc,[12] all evidencing that the reaction takes place on the central metallic cation, with the macrocycle only able to increase or decrease this reactivity by modifing the molecular orbitals.[13] A study on the reactivity of metal free naphthalocyanine towards oxygen was presented by Ottaviano et al.[14] who found that the reaction takes place on the azabridge nitrogen atoms which are saturated by H in metal-free phthalocyanine and derivatives; the two hydrogens are dislodged by the oxygen molecules binding to the phthalocyanine. Also studies on the interaction between single decker phthalocyanine and transition metal oxide surface were performed. For example, the investigation from Glaser et al.[15] showed a charge transfer from the MnO substrate to the CoPc overlayer, and a subsequent shift of the Co 2p towards lower Binding Energy (BE) due to the rehybridization of the Co and MnO orbitals, while no modifications were seen on the N and C 1s spectra. Liu and coworkers[16] showed instead that deposition of FePc over MoO_x led to oxidation of the metallic centre. All these works evidenced that the crucial location for the molecular reactivity lies on the central cation (or the N atoms saturated by hydrogens in the case of metal free Pcs). The central metallic cation has a dominant role in the charge redistribution during the charge transfer process[17] and therefore influences the charge carriers mobility.

To improve the stability of phthalocyanine based organic devices, a class of molecules that would naturally prevent the above mentioned reaction mechanism on the cation, is represented by double-decker phthalocyanine. The geometry of $LuPc_2$ is shown in Figure 1, the coordination sphere of the central Lu^{3+} cation is saturated by the eight pyrrolic nitrogen atoms. This saturation should prevent the central ion from reacting, making of this class

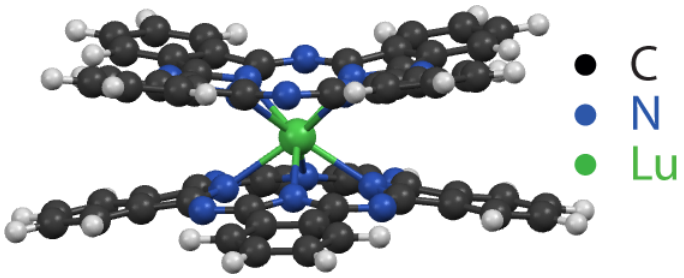

Figure 1: DFT optimized structure of an isolated $LuPc_2$ molecule.

of phthalocyanine a promising alternative to the widely used single decker ones. Only few studies were published on the reactivity of double-decker phthalocyanines[18–20] and mostly from a device point of view. For example the study of the conductivity before and after the exposition to highly oxidizing gases showed at first an increase of the conductivity due to the partial oxidation of the film[18] which produced an increased hopping possibility caused by the increased number of accepting molecules. A further oxidation led then to a decrease in conductivity, due to the increased fraction of oxidized molecules, and therefore a reduced number of accepting sites.

So far very little is known about the microcopic molecular processes leading to such reactivity; in the present study, we propose to adress this issue by investigating the reactivity of $LuPc_2$ thin films towards molecular oxygen at low temperature. Surface spectroscopies as X-ray Photoelectron Spectroscopy (XPS) and Near Edge X-ray Absorption Fine Structure Spectroscopy (NEXAFS) are the perfect tools to reveal the intimate mechanisms, as they guarantee great surface sensitivity (i.e. only the top few layers are probed), chemical selectivity and site specificity as well as information about the charge redistribution after the reaction. By combining experimental techniques and advanced Density Functional Theory (DFT) simulations, we were able to define precisely the location and energy adsorption of O_2 molecules on $LuPc_2$.

Experimental and/or Theoretical Methods

The experiment was performed at the beamline D1011 in MAX IV Laboratory in Lund at the front station.[21] The D1011 beamline is a bending magnet beamline which allows a flux of 10^{10}- 10^{11} linearly polarized (85%) photons·s^{-1}. The endstation is composed of two chambers: a preparation chamber and an analysis chamber. In both chambers the base pressure was in the low 10^{-10} mbar range. The preparation chamber was equipped with an ion gun, an e-beam heating to prepare the sample, and Low Energy Electron Diffraction (LEED). The analysis chamber was equipped with electron spectrometer (VG Scienta SES200 concentric hemispheric analyser), electron detector with partial and total electron yield for NEXAFS measurement. Au(111) single crystal was purchased by Surface Preparation Laboratory (SPL). It was cleaned by repeated cycles of sputtering and annealing until no N, C signal was seen in the NEXAFS or in the XPS spectrum. The last annealing was performed at 873 K and slowly cooled to obtain the $(\sqrt{3} \times 22)$ herringbone reconstruction,[22] which was checked by LEED.

$LuPc_2$ molecules were synthesized as reported in literature.[23,24] Before the evaporation, the crucible and the molecules were carefully outgassed at 250°C for several hours to remove the residual H_2Pc, until the base pressure was recovered. The organic layer was prepared by thermal evaporation of the molecules from a homemade Ta pocket heated by direct current. Evaporator temperature was kept around 573 K and was measured with a thermocouple coiled around the crucible. During the deposition, the sample was kept at room temperature and the total pressure was kept in the 10^{-8} mbar regime for about 30 minutes. The layer was thick enough so that no Au 4f peak was seen with the XPS ensuring a covering of at least 3 nm. The XPS data were collected with pass energy of 100 eV, and the overall resolution was about 0.1 eV. The spectra were recorded with Photon Energy (PE) of 500 eV and 450 eV for N 1s and C 1s spectra respectively. Electrons were collected in normal emission and the BE scale was calibrated on the main C 1s line, which was found at the same BE as previously published,[25,26] or on Lu $4f$ which both did not show any shift after oxygen

exposure. A mixed Shirley and linear background was subtracted from XPS data, and the data were analysed with IgorPro software and the SPANCF procedure.[27] Voigt curves with fixed Lorentzian FWMH of 0.1 eV and 0.132 eV were used for C 1s and N 1s respectively while the width of the Gaussian curve was left free to vary in the fitting procedure. The intensities have been normalized to unity on the main feature height.

NEXAFS spectra were taken in partial electron yield mode using a channel plate with a retarding voltage of 150 eV and an energy step of 50 meV for the π resonances and 100 meV for the σ resonances. The resolution E/ΔE exceeded 6000 for the N and O K-edge thresholds,[28] equivalent to a resolution of around 50 meV for N K-edge, and 80 meV for O K-edge. Two polarizations were investigated: in-plane polarization (IPP) for which the polarization E vector of the radiation was nearly parallel to the surface (misalignment of about 4°) and out-of-plane polarization (OPP). The photon energy was calibrated at the beginning and at the end of the first N K-edge spectrum with C 1s first and second order, and successive spectra were calibrated on the first π^* resonance. The spectra were first divided by the references on clean Au substrate taken at the beginning of the experiment, and then set to 0 below threshold.[29]

Oxygen with purity >99.995%, purchased by Air Liquid, was introduced through a leak valve in the preparation chamber. During the dose, the pressure was kept in the low 10^{-5} mbar.

Density Functional Theory (DFT) was employed to gain insights into the interaction between the O_2 molecule and $LuPc_2$. The computations, i.e. structure optimization and XPS simulations, were performed on single molecules and for the two molecules, i.e. O_2 adsorbed on $LuPc_2$, interacting with each other. For this purpose, the VASP package[30–32] was used with the implemented projector augmented wave method (PAW),[33] the Perdew-Burke-Ernzerhof (PBE) exchange-correlation functional[34,35] and the Tkatchenko-Scheffler (TS) dispersion correction,[36] which is required in DFT to accurately describe weakly interacting systems, e.g. such that are physisorbed. To minimize cross talk between periodic

images, the simulations cells contained 10 Å of vacuum in each direction which resulted in box sizes of at least, e.g. 25×25×16 Å^3 for a single $LuPc_2$. The interaction of $LuPc_2$ with one O_2 molecule was investigated in a two steps optimization approach and with several initial geometries. The initial geometries were pseudo-randomly generated with distances between O_2 and $LuPc_2$ ranging from 2.4 to 3.5 Å. Due to symmetry of the $LuPc_2$ structure, the initial O_2 positions were located at only one of the isoindene rings. In total, 90 initial geometries were generated with O_2 at different sites and with different orientations. Then, preoptimizations were carried out for these structures with an energy cutoff of 300 eV and a low force convergence of 0.03 eV/ Å. In step two, the six most stable structures were selected for continuation of their geometry optimization being carried out with an energy cutoff of 500 eV until all forces on the atoms were less than 0.02 eV/ Å. The isolated $LuPc_2$ and the isolated O_2 molecule were also optimized with the latter convergence criteria. For all calculations, the Brillouin zone was sampled at the Γ point only.

The adsorption energy (E_{ad}) is estimated as total energy difference between the final geometry consisting of one O_2 molecule adsorbed on one $LuPc_2$ ($E_{LuPc_2O_2}$) and the total energies of the two separated molecules individually, i.e. the total energies of the optimized single molecules E_{O_2} and E_{LuPc_2}, according to $E_{ad} = E_{LuPc_2O_2}$ - (E_{O_2} + E_{LuPc_2}).

N 1s and C 1s XPS simulations were performed with the modified PAW by Köhler[37] in VASP, which allows to relax the otherwise frozen core states. We chose to compute energy shifts in XPS via a ground state approximation for which we estimate the 1s ionization energy of a state being equal to its computed eigenvalue. In this way, computed 1s XPS signal is, however, a relative measure and only comparable to the same element within the same computational setup while absolute excitation energies cannot be obtained. Nonetheless, relative shifts in photoemission spectra, for example in C 1s, can provide information about chemical environment of atoms and changes of it which makes this approach suitable to study the interaction between $LuPc_2$ with O_2 and it allows to interpret possible changes in experimental data. We distinguish between two different shifts: i) a shift (Δ) due to

the chemical bonds within a molecule, e.g., the well-known shift of about 1.3 eV between pyrrolic and benzene C 1s signal (which is well-known for many phthalocyanines[25] from experimental measurements) and ii) a shift (δ) due to adsorption of other molecules like O_2 which is measured at the same atom before and after O_2 adsorption. We also introduce the XP range, that corresponds to the maximal difference computed for the energy position of C 1s or N 1s core levels.

Results and discussion

XPS results

Figure 2 presents the experimental XPS spectra of C 1s and N 1s (green dots for spectra (C1) and (N1)) for the as deposited $LuPc_2$ film, after a dose 3600 L O_2 (spectra (C2) and (N2)) and 90000 L O_2 (spectra (C3) and (N3)) at 90 K, respectively. The N 1s spectrum for the as deposited sample shows a main peak at 398 eV with a single shoulder at higher BE around 399 eV. The C 1s spectrum instead shows a main peak at 284.5 eV with two shoulders at higher BE. In both spectra, a shoulder appears at higher BE next to the main peak after the first oxygen dose of 3600 L ($1L = 1 \times 10^{-6}$ Torr$\times 1s$) (spectra (C2) and (N2)), that increases further after the second dose of 90000 L (spectra (C3) and (N3)). The measurements at 90 K were followed by a warming up to RT that revealed a complete restoration of the XPS spectra for both carbon and nitrogen species (see Supporting Information) and also NEXAFS at the nitrogen K-edge. The original NEXAFS was already retrieved for a temperature around 120 K (not shown), evidencing the weak bonding between the molecular oxygen and the $LuPc_2$ molecules which affects both C 1s and N 1s. To go further in the analysis of the XPS, spectral components for the N 1s and C 1s peaks have been extracted and are displayed in Figure 2. Fitting results are detailed in Tab. 1 and Tab. 2 for the N 1s and C 1s levels respectively and are similar to already published data[25,26] on pristine $LuPc_2$ films, except for the resolution which is inferior in our case.

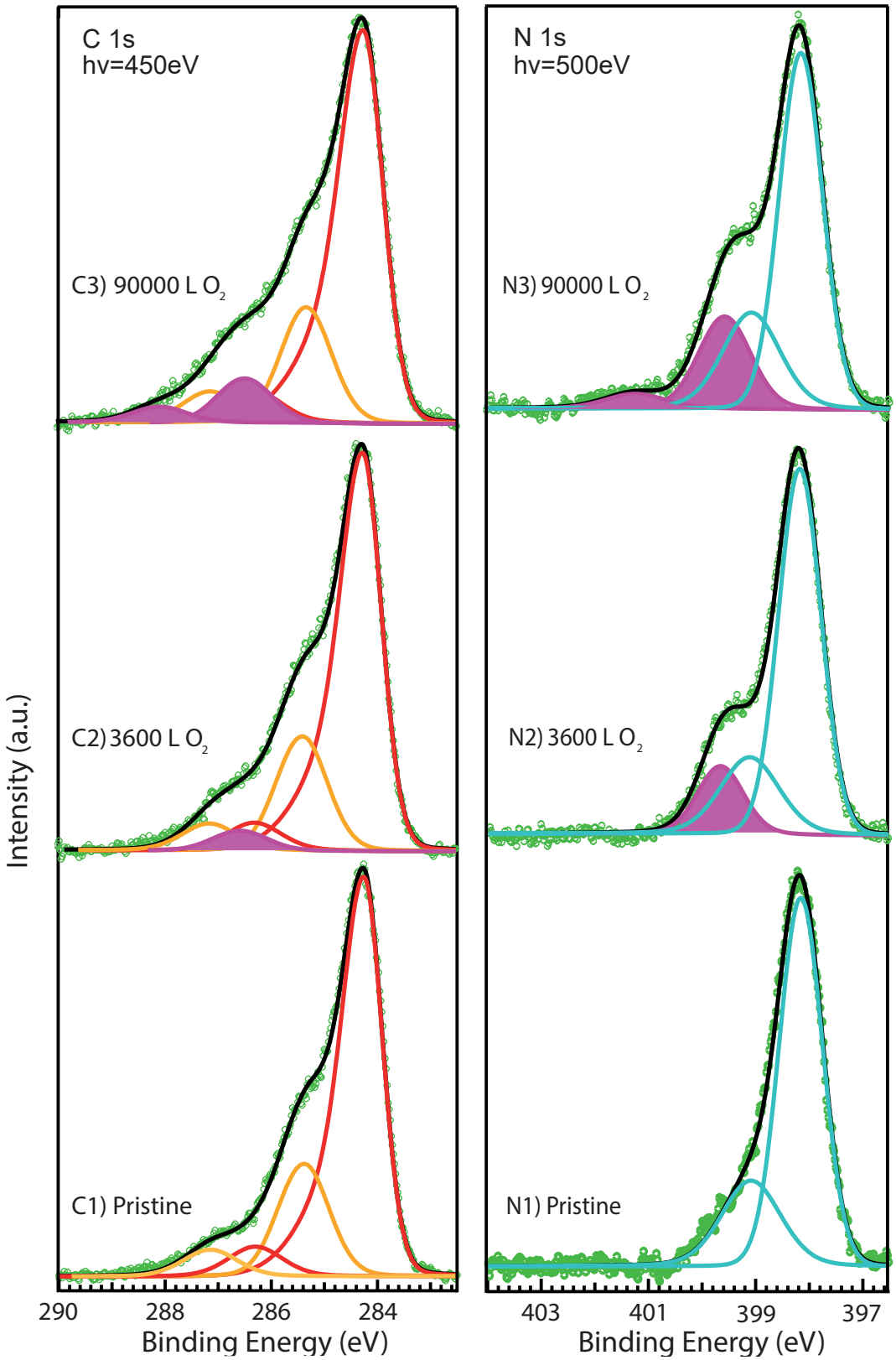

Figure 2: XPS spectra of C 1s (left) and N 1s (right) for increasing oxygen exposure at 90 K on a $LuPc_2$ film.

Table 1: Peak fitting parameters of the N 1s spectra including BE, Area (normalized on the height of the first peak). $Sh-up$ **indice refers to shake-up satellite.**

Peak	Position (eV)	Area
Clean		
N 1s	398.15	0.95
N $1s_{sh\text{-}up}$	399.10	0.30
After 3600 L of O_2		
N 1s	398.15	0.95
N $1s_{sh\text{-}up}$	399.10	0.30
N+O	399.65	0.19
After 90000 L of O_2		
N 1s	398.15	0.90
N $1s_{sh\text{-}up}$	399.10	0.35
N+O	399.55	0.30
N+$O_{sh\text{-}up}$	401.25	0.05

For the N 1s level in the pristine $LuPc_2$ film (Figure 2 spectrum (N1)), the main peak is composed of both the azabridge and the pyrrolic nitrogen atoms contributions, which are too close (30 meV) to be resolved,[38] and their associated shake-up at 399.10 eV. No asymmetry is taken into account while fitting the N 1s peak as the two peaks are supposed to have the same intensity (i.e. same number of atoms contributing to the peak). After the first oxygen exposition (Figure 2 spectrum (N2)), a third component is evidenced, at BE of 399.65 eV, referred to as N+O. After the second exposition (Figure 2 (N3)), an increase of this N+O component is clearly observed together with the appearance of a second additional component at 401.25 eV, referred to as N+O_{sh-up}.

For the C 1s level in the pristine film (Figure 2 spectrum (C1)) the main peak is mostly due to contributions from benzenic carbon found at 284.25 eV. A slight asymmetry is used to take into account for the contribution arising from the two slightly different carbon atoms: the four linked directly to pyrrolic carbons and the four bound to other benzenic carbon as discussed in ref.[39] The shoulder at higher BE is composed by contributions from pyrrolic carbons at 285.40 eV and shake-up of the benzenic carbon[39] at 286.30 eV. The last shoulder

Table 2: Peak fitting parameters of the C 1s spectra including BE and Area. $Sh-up$ indice refers to shake-up satellite.

Peak	Position (eV)	Area
As deposited		
C_{benz}	284.25	1.35
$C_{benz/sh-up}$	286.30	0.10
C_{pyrr}	285.40	0.3
$C_{pyr/sh-up}$	287.15	0.10
After 3600 L of O_2		
C_{benz}	284.25	1.35
$C_{benz/sh-up}$	286.30	0.10
C_{pyrr}	285.40	0.35
$C_{pyr/sh-up}$	287.15	0.10
C+O	286.55	0.05
After 90000 L of O_2		
C_{benz}	284.25	1.45
$C_{benz/sh-up}$	286.30	0.10
C_{pyrr}	285.35	0.35
$C_{pyr/sh-up}$	287.15	0.10
C+O	286.50	0.15
$C+O_{sh-up}$	288.10	0.05

is due to the shake-up of the pyrrolic carbon main peak, found at 287.15 eV. After the first oxygen exposition (Figure 2 spectrum (C2)) a fifth component is present, at BE of 286.55 eV, called C+O. After the 90000 L O_2 dose, the C+O peak increases in intensity, and also a sixth peak is appearing at 288.10 eV, referred to as $C+O_{sh-up}$. No changes could be observed in the Lu 3d and 4f peaks. The XPS results reveal the presence of additional features in the N 1s and C 1s core levels whose intensities increase with the oxygen dose at 90 K.

DFT results

Figure 3 shows the six most stable DFT optimized structures of one O_2 molecule adsorbed on one $LuPc_2$ labeled from a) to f). In Tab. 3, the adsorption energies of the structures shown in Figure 3 are given together with their O_2 binding distances. For these structures, the computed adsorption energies are found between -270 and -200 meV, the distances between O_2 and the Pc rings are in the range of 3.1 to 3.7 Å and the distances between Lu ion

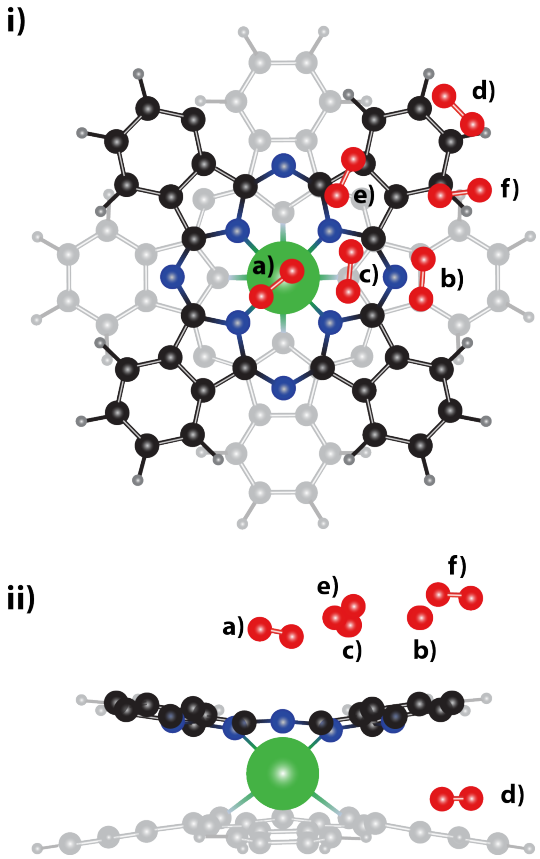

Figure 3: Optimized adsorption structures, superimposed onto each other, a) to f) of O_2 on $LuPc_2$ in i) top view and ii) side view.

and O_2 are larger than 4.1 Å. Both adsorption energies and adsorption distances indicate physisorption. Also, the large distances to Lu imply that the metal ion does not directly interact with the O_2 molecule for all computed structures. Interestingly, most energy differences between the adsorption sites are rather small, less than 70 meV, while the adsorption sites are distributed over almost the whole isoindole ring. In addition, the O_2 molecule interacts stronger with $LuPc_2$ towards the center of the plateau, i.e. in vicinity of the pyrrolic ring. This points towards a flat adsorption potential over the Pc plateau with the strongest interaction around its central region. Only when O_2 is above the Pc plane and behind the edge of the Pc plateaus, the adsorption energies drop significantly below 110 meV (structures not shown). It should be noted that O_2 in structure d) is at the edge of the Pc but between the two plateaus which results in 220 meV binding strength.

Table 3: Adsorption energies (E_{ad}) and binding distances between O_2 and the Lu ion (d(O_2-Lu)), and O_2 and the Pc plateaus (d(O_2-Pc)) for structures a) to f) shown in Figure 3.

Structure according to Figure 3	E_{ad} (meV)	d_{O_2-Pc} (Å)	d_{O_2-Lu} (Å)
a)	270	3.4	4.1
b)	250	3.3	6.3
c)	220	3.1	5.0
d)	220	3.3	7.4
e)	210	3.3	5.6
f)	200	3.7	7.9

Table 4 shows the computed XP range, i.e. the difference between the largest and the smallest values of binding energy for the different atoms. We distinguish the XP range among N atoms (XP_N) and C atoms (XP_C). In the isolated $LuPc_2$, XP_N is less than 50 meV, which is in line with the experimental observation of a single peak for the nitrogen inequivalent atoms. Whereas, XP_C is estimated as 1.8 eV which overestimates the experimental C 1s chemical shift between the pyrrolic and the benzene atoms by about 0.5 eV. This overestimation is likely caused by the ground state approach used to compute the relative energy shifts in the XPS. Nonetheless, as we focus on the O_2 adsorption induced changes, the overestimated C 1s XP range is not expected to affect the conclusions. In Tab 4, the

simulated XP range results of structure c) and e) are highlighted, because the presence of the O_2 molecule in vicinity of pyrrolic N and C atoms causes a significant increase of the XP range and therefore induces a large XPS energy shift compared to the isolated $LuPc_2$ and to the other structures, i.e. a), b), d) and f). The increased XP range in structures c) and e) is mostly caused by large energy shifts of several hundreds of meV seen in 1s levels of C and N atoms closest to the adsorbed O_2 and to a minor extent to small shifts in other atoms. DFT results indicate that physorption rather than chemisorption is governing the adsorption of oxygen at low temperature and show that photoemission core level spectra are more affected when oxygen molecules lie closer to pyrrolic groups.

Table 4: XP ranges for N 1s (XP_N) and C 1s (XP_C) levels of the single $LuPc_2$ and O_2 optimized structures according to Figure 3. Large values leading to XPS shifts are highlighted.

	XP_N (eV)	XP_C (eV)
$LuPc_2$	0.044	1.759
a)	0.025	1.755
b)	0.033	1.769
c)	**0.378**	**2.584**
d)	0.044	1.789
e)	**0.466**	**2.090**
f)	0.026	1.772

NEXAFS results

In Figure 4 (A), the NEXAFS spectra of N K-edge taken with two light polarizations are shown for the pristine $LuPc_2$ film and after 90000 L of O_2; in-plane polarization (IPP) is displayed in black and out-of-plane polarization (OPP) in light blue. Two regions can be distinguished in the spectra: below and above the ionization threshold around 405 eV. The region below PE of 405 eV, originates from N 1s $\rightarrow \pi^*$ transitions, while above 405 eV, transitions from N 1s $\rightarrow \sigma^*$ are probed. For the IPP polarization, the two peaks at 398.1 eV and 400 eV originate from azabridge and pyrrolic nitrogen resonances respectively, for further assignment of the NEXAFS resonances of $LuPc_2$ the reader can refer to the work by

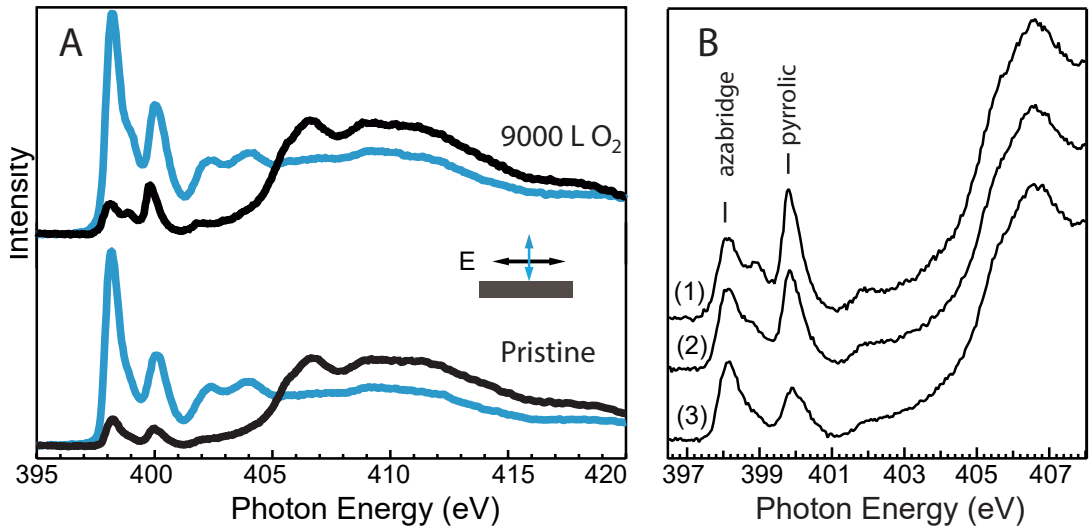

Figure 4: A : NEXAFS spectra at the N K-edge for incoming beam polarized almost parallel (incidence angle= 4°) to the plane (IPP geometry, black) and perpendicular to the plane (OP polarization, light blue) for the $LuPc_2$ pristine film and for the film exposed to 90000 L of O_2, both taken at T=90 K; B : Zoom on the $\pi^\star$ transition in the in-plane geometry for the pristine sample (1), after 3600 L of O_2 at 90 K (2) and after 90000 L of O_2 at 90 K (3).

Bidermane et al.[25] The NEXAFS spectra show a clear dichroism, with the π^* (σ^*) resonances dominating in the out of plane (inplane) polarization for the pristine $LuPc_2$ film. As the NEXAFS cross section is strongly dependent on the mutual orientation of the light polarization and the final orbital,[29] this is a clear indication that the molecules lie flat on the substrate for this thickness (>3 nm) . The dichroism is conserved after the 90000 L O_2 dose, confirming that the molecules still lie flat after the dose and the almost unchanged intensity ratio between the σ^* and π^* resonances before and after the deposition is due to a limited rehybridization of the molecular orbitals after interaction with O_2. After the oxygen dose, a new peak is visible at 399 eV in the IPP geometry and also the intensity of the $\pi^\star$ resonance at 400 eV, corresponding to the pyrrolic atom, becomes stronger, as clearly seen in Figure 4 (B). The origin of the new feature will be discussed in the next section. Note that the possibility of a reaction with condensed water, atomic oxygen or O_3 (created by the x-ray irradiation) was ruled out thanks to NEXAFS measurement on the oxygen K-edge (see Supporting Information).

From the NEXAFS data, it is possible to evidence that the $LuPc_2$ molecules lie flat on the surface before and after the oxygen dose, and that a perturbation of the electronic structure is induced by the oxygen adsorption at low temperature.

Discussion

The first adsorption mechanism evidenced from the experiment, relies in the weakness of the $LuPc_2$-O_2 bond, shown by the low desorption temperature of around 120 K and the complete restoration of the photoemission spectra after desorption. This behavior points towards a physisorption rather than a chemisorption of the oxygen molecule on the $LuPc_2$ film. This hypothesis is corroborated by the analysis of the binding energy of the XPS additional peaks. No literature could be found on this specific system, but the N+O feature at 399.65 eV in the N 1s XPS spectrum can not be related to N atoms directly bound to oxygen which are usually found for BE around 401.3 eV.[40–42] The DFT results give further evidence of weak interaction, i.e. physisorption, between O_2 and $LuPc_2$ with adsorption energies of 270 meV or less and adsorption distances of at least 3.1 Å.

The preferential adsorption sites are deduced from the combined analysis of XPS core levels and DFT simulations. There are no studies reporting on similar systems but analogies can be drawn based on N 1s and C 1s binding energies. Whereas BE of about 401 eV is found for N atoms chemically bound to oxygen, the BE falls around 399 eV[43–45] for N atoms in the vicinity of carbonyl groups, suggesting such kind of proximity in our system. In the case of the C 1s spectrum the additional peak can be related to a C-O bond in polymers, in small molecules or on graphite[40,42,46–50] but again, no literature could be found on this specific or closely related systems. Therefore, the analysis of the BE in the XPS data suggest the adsorption of the oxygen molecule close to carbon atoms, and most likely the pyrrolic carbon atoms, since N 1s is largely affected. This finding is supported by our DFT calculations for which the two adsorption geometries presenting the larger changes in BE are obtained for oxygen molecules adsorbed near or on a pyrrole ring. However, our DFT results do not

address the attachment of more than one O_2 molecule at one $LuPc_2$ which may cause slight changes in the adsorption energies. Because the XPS measurements detect large shifts in both N 1s and C 1s resonances due to O_2 adsorption, which was not seen in the simulated XPS for the most stable adsorption site computed (a), it can be assumed that other effects (e.g. vibrations) prevent the structure a) from being the most stable structure or/and that several O_2 molecules can adsorb on one $LuPc_2$ simultaneously, molecules in a) configuration leaving the experimental spectra unaffected. Then, other structures must be present on the $LuPc_2$ to account for experimental findings. In this regard, structures c) and e) give qualitative agreement between computed and experimental XPS changes. Moreover, the adsorption energies of c) and e) are only slightly larger than for a), i.e. 50 and 60 meV, respectively. The tilt of molecules in the stacking with respect to the surface could also play a role in the reaction making the configuration (f) accessible to oxygen molecules for an edge-on orientation of the molecules. Unfortunately, this configuration is not expected to lead to an additional feature in the XPS spectrum and more appropriate measurements such as transport would be more relevant to evidence the influence of the stacking on the reactivity.

Therefore, it can be concluded that at least one of these configuration is present in the experiment and that O_2 is adsorbed in the vicinity of the pyrrole ring.

A detailed understanding of the electronic structure derived from the XPS and NEXAFS measurements can be drawn. Looking more carefully at the zoom of the IPP NEXAFS in the Figure 4 (B), a new peak arises at PE (Photon Energy) of 398.9 eV, separated by 0.8 eV from the first π^* resonance at 398.1 eV is observed for increasing oxygen doses. Furthermore the intensity of the second $\pi^\star$ at 400 eV resonance increases with respect to the first $\pi^\star$ resonance. This inversion in the intensities after the O_2 exposition can not be explained by a slight tilt of one of the C-N bond after the oxygen adsorption since in the OPP no changes are seen in the ratio between the second $\pi^\star$ at 400 eV and the first $\sigma^\star$ transition at 406 eV

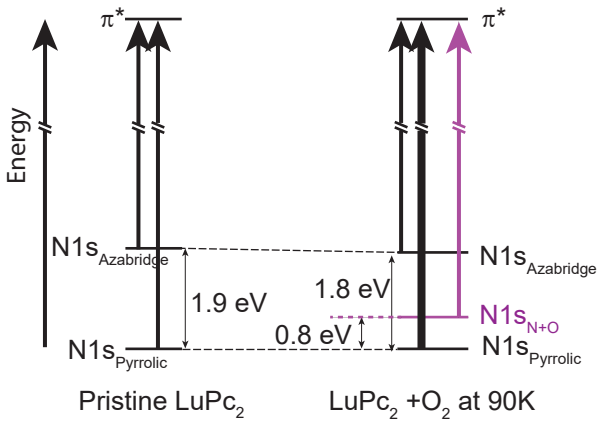

Figure 5: Energy diagram of the allowed NEXAFS transitions for the IPP geometry before (left) and after (right) oxygen exposure derived from XPS and NEXAFS.

for the spectra collected before and after the exposition to oxygen. Instead, as the NEXAFS peaks intensity is strongly dependent on the occupancy of the final state orbitals and their energy density, this is probably an evidence of charge withdrawal[51] from the molecule to the oxygen. The effect is clearly seen in the IPP but not in the OPP (see Figure 4 (A)), and it has to be remembered that in this polarization the two π^* resonances can be attributed to different N atoms: the first one is mostly due to $N_{azabridge}$ →LUMO, while the second one is mostly due to $N_{pyrrolic}$ →LUMO.[25] This finding is reinforced by the intensity and the BE of the additional component in the N 1s spectra (Figure 2 spectrum (N3)), which suggests a strong charge withdrawal from the N atoms due to the spatial proximity. Both XPS and NEXAFS strongly suggest a charge withdrawal from the pyrrolic nitrogen, where most of the LUMO is localized. The nature of the additional component that appears at 398.9 eV can be understood by a combined interpretation of the XPS and NEXAFS spectra and is depicted by the diagram in Figure 5. It is assigned to the same transition N 1s → π^* as the other two resonances, but from the nitrogen atom close to the oxygen adsorption site (illustrated by violet arrow and responsible for the N+O component in the XPS spectrum). The oxygen adsorption lifts the degeneracy between the 8 equal pyrrolic nitrogens, as shown by the additional peak in the XPS spectrum, which is relative to a chemically inequivalent N atom, giving rise to an additional transition in the NEXAFS spectrum. This effect was

already shown by Solomon and coworkers on a similar system.[52] The lower energy (PE) of the additional peak in the NEXAFS spectrum with respect to the energy (BE) of the N+O component in the XPS spectrum might be due to the better screening of the final state in the NEXAFS process which retains the electron around the molecule, allowing it to still screen the core hole.[29] Surprisingly, the physisorption of molecular oxygen induces a reversible charge transfer from the nitrogen atom of the pyrrolic group to the oxygen. Such intriging behavior would require further calculations to fully understand the underlying mechanisms.

Conclusion

Thanks to a combined theoretical and experimental investigation, we are able to draw a microscopic picture for the adsorption of molecular oxygen on $LuPc_2$ film. We demonstrate that double-decker phthalocyanines of lutetium are poorly reactive to molecular oxygen and appears as a high tolerant organic molecules leaving the Lu ion unaffected by the process. The experimental XPS data supported by computed XPS carried out for the first time on individual molecules, confirm that oxygen molecules weakly physisorb nearby the pyrrolic nitrogen of the ligand plateau.

The high tolerance of double-decker phthalocyanine towards molecular oxygen can open promising perspectives for the design of novel materials to be applied in the next generation of organic based electronic devices operating under ambient conditions.

Acknowledgments

We are grateful to D1011 beamline staff for providing support and assistance during the beamtime. We acknowledge the financial support from the Knut and Alice Wallenberg foundation, the European Union Seventh Framework Programme under grant agreement n° 607232 THINFACE, the Swedish Research Council (Grant 2014-3776) and the Swedish National Infrastructure for Computing (SNIC).

Supporting Information

XPS spectra of C1s and N1s for increasing dose of oxygen and after annealing at room temperature.

NEXAFS at the O K edge.

References

(1) Kaltenbrunner, M.; White, M. S.; Glowacki, E. D.; Sekitani, T.; Someya, T.; Sariciftci, N. S.; Bauer, S. Ultrathin and Lightweight Organic Solar Cells with High Flexibility. *Nat. Commun.* **2012**, *3*, 770.

(2) Jean, J.; Wang, A.; Bulovic, V. In Situ Vapor-Deposited Parylene Substrates for Ultra-Thin, Lightweight Organic Solar Cells. *Org. Electron.* **2016**, *31*, 120 – 126.

(3) Nakanotani, H.; Higuchi, T.; Furukawa, T.; Masui, K.; Morimoto, K.; Numata, M.; Tanaka, H.; Sagara, Y.; Yasuda, T.; Adachi, C. High-Efficiency Organic Light-Emitting Diodes With Fluorescent Emitters. *Nat. Commun.* **2014**, *5*.

(4) Bof Bufon, C. C.; Vervacke, C.; Thurmer, D. J.; Fronk, M.; Salvan, G.; Lindner, S.; Knupfer, M.; Zahn, D. R. T.; Schmidt, O. G. Determination of the Charge Transport Mechanisms in Ultrathin Copper Phthalocyanine Vertical Heterojunctions. *J. Phys. Chem. C* **2014**, *118*, 7272–7279.

(5) Zhao, D.; Huang, W.; Qin, Z.; Wang, Z.; Yu, J. Emission Spectral Stability Modification of Tandem Organic Light-Emitting Diodes through Controlling Charge-Carrier Migration and Outcoupling Efficiency at Intermediate/Emitting Unit Interface. *ACS Omega* **2018**, *3*, 3348–3356.

(6) De Arco, L. G.; Zhang, Y.; Schlenker, C. W.; Ryu, K.; Thompson, M. E.; Zhou, C.

Continuous, Highly Flexible, and Transparent Graphene Films by Chemical Vapor Deposition for Organic Photovoltaics. *ACS Nano* **2010**, *4*, 2865–2873.

(7) Seemann, A.; Sauermann, T.; Lungenschmied, C.; Armbruster, O.; Bauer, S.; Egelhaaf, H. J.; Hauch, J. Reversible and Irreversible Degradation of Organic Solar Cell Performance by Oxygen. *Sol. Energy* **2011**, *85*, 1238–1249.

(8) Volonakis, G.; Tsetseris, L.; Logothetidis, S. Impurity-related Degradation in a Prototype Organic Photovoltaic Material: A First-principles Study. *Org. Electron.* **2013**, *14*, 1242–1248.

(9) Lessmann, R.; Hong, Z.; Scholz, S.; Maennig, B.; Riede, M. K.; Leo, K. Aging of Flat Heterojunction Zinc Phthalocyanine/Fullerene C-60 Organic Solar Cells. *Org. Electron.* **2010**, *11*, 539–543.

(10) Sedona, F.; Di Marino, M.; Forrer, D.; Vittadini, A.; Casarin, M.; Cossaro, A.; Floreano, L.; Verdini, A.; Sambi, M. Tuning the Catalytic Activity of Ag(110)-supported Fe Phthalocyanine In the Oxygen Reduction Reaction. *Nat. Mater.* **2012**, *11*, 970–977.

(11) Lozzi, L.; Picozzi, S.; Santucci, S.; Cantalini, C.; Delley, B. Photoemission and Theoretical Investigations on NO_2 Doping of Copper Phthalocyanine Thin Films. *J. Electron Spectrosc. Relat. Phenom.* **2004**, *137*, 101–105.

(12) Flechtner, K.; Kretschmann, A.; Steinrueck, H.-P.; Gottfried, J. M. NO-Induced Reversible Switching of the Electronic Interaction between a Porphyrin-Coordinated Cobalt Ion and a Silver Surfacee. *J. Am. Chem. Soc.* **2007**, *129*, 12110–12111.

(13) Flyagina, I. S.; Hughes, K. J.; Pourkashanian, M.; Ingham, D. B. DFT Study of the Oxygen Reduction Reaction on Iron, Cobalt and Manganese Macrocycle Active Sites. *Int. J. Hydrogen Energy* **2014**, *39*, 21538–21546.

(14) Ottaviano, L.; Lozzi, L.; Santucci, S. Interaction of Naphthalocyanine with Oxygen and with Si(111) 7x7: An in-situ X-ray Photoelectron Spectroscopy Study. *Surf. Sci.* **1999**, *431*, 242–251.

(15) Glaser, M.; Peisert, H.; Adler, H.; Ayguel, U.; Ivanovic, M.; Nagel, P.; Merz, M.; Schuppler, S.; Chasse, T. Electronic Structure at Transition Metal Phthalocyanine-Transition Metal Oxide Interfaces: Cobalt Phthalocyanine on Epitaxial MnO Films. *J. Chem. Phys.* **2015**, *142*.

(16) Liu, L.; Zhang, W.; Guo, P.; Wang, K.; Wang, J.; Qian, H.; Kurash, I.; Wang, C.-H.; Yang, Y.-W.; Xu, F. A Direct Fe-O Coordination at the FePc/MoOx Interface Investigated by XPS and NEXAFS Spectroscopies. *Phys. Chem. Chem. Phys.* **2015**, *17*, 3463–3469.

(17) Chen, S.; Ma, J. Charge Transport in Stacking Metal and Metal-Free Phthalocyanine Iodides. Effects of Packing, Dopants, External Electric Field, Central Metals, Core Modification, and Substitutions. *J. Comput. Chem.* **2009**, *30*, 1959–1972.

(18) Passard, M.; Blanc, J. P.; Maleysson, C. Gaseous Oxidation and Compensating Reduction of Lutetium Bis-phthalocyanine and Lutetium Phthalo-naphthalocyanine Films. *Thin Solid Films* **1995**, *271*, 8–14.

(19) Yamana, M.; Kashiwazaki, N. Effects of Heat Treatment on Oxidative Gas Adsorption for Lead Naphthalocyanine Thin Films. *Sens. Actuators B* **1997**, *40*, 237–241.

(20) De Saja, J.; Rodriguez-Mendez, M. Sensors Based on Double-Decker Rare Earth Phthalocyanines. *Adv. Colloid Interface Sci.* **2005**, *116*, 111.

(21) Nyholm, R.; Svensson, S.; Nordgren, J.; Flodström, A. A Soft-x-ray Monochromator for the Max Synchrotron Radiation Facility. *Nucl. Instrum. Methods Phys. Res., Sect. A* **1986**, *246*, 267–271.

(22) Barth, J. V.; Brune, H.; Ertl, G.; Behm, R. J. Scanning Tunnelling Microscopy Observations on the Reconstructed Au(111) Surface: Atomic Structure, Long-range Superstructure, Rotational Domains, and Surface Defects. *Phys. Rev. B* **1990**, *42*, 9307–9318.

(23) Bouvet, M.; Simon, J. Electrical-properties of Rare-earth Bisphthalocyanine and Bisnaphthalocyanine Complexes. *Chem. Phys. Lett.* **1990**, *172*, 299–302.

(24) Clarisse, G.; Riou, M. T. Synthesis and Characterization of some Lanthanide Phthalocyanines. *Inorg. Chim. Acta* **1987**, *130*, 139–144.

(25) Bidermane, I.; Lüder, J.; Boudet, S.; Zhang, T.; Ahmadi, S.; Grazioli, C.; Bouvet, M.; Rusz, J.; Sanyal, B.; Eriksson, O. et al. Experimental and Theoretical Study of Electronic Structure of Lutetium Bi-phthalocyanine. *J. Chem. Phys.* **2013**, *138*.

(26) Toader, M.; Knupfer, M.; Zahn, D. R. T.; Hietschold, M. Initial Growth of Lutetium(III) Bis-phthalocyanine on Ag(111) Surface. *J. Am. Chem. Soc.* **2011**, *133*, 5538–5544.

(27) Kukk, E. E. Kukk, Spectral Analysis by Curve Fitting Macro Package SPANCF 2000. http://www.geocities.com/ekukk.

(28) Vinogradov, A. S.; Fedoseenko, S. I.; Krasnikov, S. A.; Preobrajenski, A. B.; Sivkov, V. N.; Vyalikh, D. V.; Molodtsov, S. L.; Adamchuk, V. K.; Laubschat, C.; Kaindl, G. Low-lying Unoccupied Electronic States in 3d Transition-metal Fluorides Probed by NEXAFS at the F 1s Threshold. *Phys. Rev. B* **2005**, *71*.

(29) Stöhr, J. *NEXAFS Spectroscopy*; Springer-Verlag Berlin Heidelberg, 2003.

(30) Kresse, G.; Hafner, J. Ab initio Molecular Dynamics for Liquid Metals. *Phys. Rev. B* **1993**, *47*, 558–561.

(31) Kresse, G.; Furthmüller, J. Efficient Iterative Schemes for ab initio Total-energy Calculations using a Plane-wave Basis Set. *Phys. Rev. B* **1996**, *54*, 11169–11186.

(32) Kresse, G.; Furthmüller, J. Efficiency of ab-initio Total Energy Calculations for Metals and Semiconductors using a Plane-wave Basis Set. *Comput. Mater. Sci.* **1996**, *6*, 15–50.

(33) Kresse, G.; Joubert, D. From Ultrasoft Pseudopotentials to the Projector Augmented-wave Method. *Phys. Rev. B* **1999**, *59*, 1758–1775.

(34) Perdew, J. P.; Burke, K.; Ernzerhof, M. Generalized Gradient Approximation Made Simple. *Phys. Rev. Lett.* **1996**, *77*, 3865–3868.

(35) Perdew, J. P.; Burke, K.; Ernzerhof, M. Generalized Gradient Approximation Made Simple [Phys. Rev. Lett. 77, 3865 (1996)]. *Phys. Rev. Lett.* **1997**, *78*, 1396–1396.

(36) Tkatchenko, A.; Scheffler, M. Accurate Molecular van der Waals Interactions from Ground-State Electron Density and Free-atom Reference Data. *Phys. Rev. Lett.* **2009**, *102*, 073005.

(37) Köhler, L.; Kresse, G. Density Functional Study of CO on Rh(111). *Phys. Rev. B* **2004**, *70*, 165405.

(38) Bidermane, I.; Lüder, J.; Ahmadi, S.; Grazioli, C.; Bouvet, M.; Brena, B.; Mårtensson, N.; Puglia, C.; Witkowski, N. When the Grafting of Double Decker Phthalocyanines on Si(100)-2 x 1 Partly Affects the Molecular Electronic Structure. *J. Phys. Chem. C* **2016**, *120*, 14270–14276.

(39) Brena, B.; Luo, Y.; Nyberg, M.; Carniato, S.; Nilson, K.; Alfredsson, Y.; Ahlund, J.; Martensson, N.; Siegbahn, H.; Puglia, C. Equivalent Core-hole Time-dependent Density Functional Theory Calculations of Carbon 1s Shake-up States of Phthalocyanine. *Phys. Rev. B* **2004**, *70*.

(40) Bouvet, M.; Leroy, A.; Simon, J.; Tournilhac, F.; Guillaud, G.; Lessnick, P.; Maillard, A.; Spirkovitch, S.; Debliquy, M.; de Haan, A. et al. Detection and Titration of

Ozone using Metallophthalocyanine Based Field Effect Transistors. *Sens. Actuators B* **2001**, *72*, 86–93.

(41) Dash, K. C.; Folkesson, B.; Larsson, R.; Mohapatra, M. An XPS Investigation on a Series of Schiff-base Dioxime Ligands and Cobalt Complexes. *J. Electron. Spectrosc. Relat. Phenom.* **1989**, *49*, 343–357.

(42) Hueso, J. L.; Espinos, J. P.; Caballero, A.; Cotrino, J.; Gonzalez-Elipe, A. R. XPS Investigation of the Reaction of Carbon with NO, O-2, N-2 and H2O Plasmas. *Carbon* **2007**, *45*, 89–96.

(43) Clegg, R. S.; Hutchison, J. E. Hydrogen-bonding, Self-assembled Monolayers: Ordered Molecular Films for Study of Through-peptide Electron Transfer. *Langmuir* **1996**, *12*, 5239–5243.

(44) Baumgarten, E.; Fiebes, A.; Stumpe, A.; Ronkel, F.; Schultze, J. W. Synthesis and Characterization of a New Platinum Supported Catalyst Based on Poly-(acrylamide-co- 3-(acryloylamino)propyltrimethylammoniumchloride) as Carrier. *J. Mol. Catal. A: Chem.* **1996**, *113*, 469–477.

(45) Lee, T. H.; Rabalais, J. W. X-ray Photoelectron Spectra and Electronic Structure of some Diamine Compounds. *J. Electron. Spectrosc. Relat. Phenom.* **1977**, *11*, 123–127.

(46) Grunze, M.; Lamb, R. N. Adhesion of Vapor Phase Deposited Ultra-thin Polyimide Films on Polycrystalline Silver. *Surf. Sci.* **1988**, *204*, 183–212.

(47) Marchant, R. E.; Zhao, Q.; Anderson, J. M.; Hiltner, A. Degradation of a Poly(ether Urethane Urea) Elastomer: Infra-red and XPS Studies. *Polymer* **1987**, *28*, 2032–2039.

(48) Steiner, U. B.; Caseri, W. R.; Suter, U. W.; Rehahn, M.; Schmitz, L. Ultrathin Layers of Low and High-molecular-weight Imides on Gold and Copper. *Langmuir* **1993**, *9*, 3245–3254.

(49) Gervais, M.; Douy, A.; Gallot, B. Surface Analysis of Lipopeptides using X-ray Photoelectron Spectroscopy: I. Lipopeptides with Polysarcosine Peptidic Chains. *J. Colloid Interf. Sci.* **1988**, *125*, 146–154.

(50) Sundberg, P.; Andersson, C.; Folkesson, B.; Larsson, R. On the XPS Spectra of some Carbonyl Complexes and the Effective Charge of the Metal and Ligand Atoms. *J. Electron. Spectrosc. Relat. Phenom.* **1988**, *46*, 85–92.

(51) Shariati, M.-N.; Lüder, J.; Bidermane, I.; Ahmadi, S.; Güthelid, E.; Palmgren, P.; Sanyal, B.; Eriksson, O.; Piancastelli, M. N.; Brena, B. et al. Photoelectron and Absorption Spectroscopy Studies of Metal-free Phthalocyanine on Au(111): Experiment and Theory. *J. Phys. Chem. C* **2013**, *117*, 7018–7025.

(52) Solomon, J. L.; Madix, R. J.; Stöhr, J. Orientation and Absolute Coverage of Benzene, Aniline, and Phenol on Ag(110) Determined by NEXAFS and XPS. *Surf. Sci.* **1991**, *255*, 12–30.

TOC Graphic